Modelling of a continuous veneer drying unit of industrial scale and model-based ANOVA of the energy efficiency

Dmitry Gradov[a], Yusuf Oluwatoki Yusuf[b], Jussi Ohjainen[c], Jarkko Suuronen[a], Roope Eskola[c], Lassi Roininen[a], Tuomas Koiranen[a]

[a] *School of Engineering Science, Lappeenranta-Lahti University of Technology (LUT), P.O.Box 20, FI-53851 Lappeenranta, Finland*
[b] *Faculty of Information Technology and Communication Sciences, Tampere University, P.O. Box 1001, FI-33014 Tampere, Finland*
[c] *Research and Development Department, Raute Oyj, P.O. Box 69, FI-15551 Nastola, Finland*

Abstract

Drying, a crucial step in process engineering aimed at producing optimal product moisture content, has evolved over time from batch processing methods to continuous processing alternatives. Continuous drying methods offer uniform moisture content of the product at lower operational cost. In this study, a continuous veneer drying model was developed based on mass and energy balances. The simulated veneer dryer is a semi-automatic machine designed to maximise the drying process efficiency via control mechanisms such as the veneer transport rate, fan speed, opening angle of the inlet and outlet dampers, and radiator temperature. In the dryer, veneer plates are conveyed horizontally through the number of connected chambers where hot air is blown transversely. The optimal drying process is dynamically maintained via the Proportional–integral–derivative controllers, manipulating the rate of the damper lids opening, that are connected to the sensors monitoring the air properties in the chambers of the drying unit. The model-based sensitivity analysis ANOVA was carried out for energy optimisation purposes. The analysis outcomes indicated that radiator temperature, initial moisture content of veneer sheets and conveyor speed are the most influential parameters affecting the drying rate. Automatic control of damper lids provides optimal temperature and moisture content of drying environment at lower energy costs.

Keywords: Continuous veneer dryer, heat and mass transfer, process and automation modelling, ANOVA, energy analysis, process optimisation.

1. Introduction

Veneers are highly demanded construction materials due to their remarkable properties such as aesthetically pleasing appearance, light weight, strength, shape stability, soundproof and low heat conduction properties. The quality of veneer sheets is moisture dependent, which should be within the optimal range for gluing. Optimal moisture content varies depending on wood type, composition of glue, panel type and other factors. Demirkir et al. (2013) state that the optimal moisture content of veneer sheets should be below 7%, whereas Ozsahin & Aydin (2014), who used a neural network on experimental data to predict the optimal veneer drying temperature for good bonding, claim that the moisture should be about 3%. In the case of over drying, unconditioned veneer plates tend to cause poor gluing due to insufficient absorption of glue aqueous component. However, high moisture content decreases the glue viscosity, which, in turn, can cause veneer sheet misalignment during hot pressing due to high shear stress (Christiansen, 1994; Colbeck et al., 1962). Recently, Ozsahin & Aydin (2014) used neural network on experimental data to predict the optimal veneer drying temperature for good bonding in the process of manufacturing plywood panels.

Email address: dmitry.gradov@lut.fi (Dmitry Gradov)

According to Johnsson et al. (2019),improving energy efficiency in wood processing industry is recognised as one of the most crucial actions for mitigating the climate change. Convective drying in veneer manufacture is a critical stage from the energy consumption perspective as it is responsible for up to 70% of the total energy consumption of plywood production (Baldwin, 1995; Aydin & Colakoglu, 2005). Moreover, plywood drying alone has been estimated to contribute more than 30% to the global warming potential of total plywood production in China, which is equivalent to 6.3 tons of emitted CO_2 per cubic meter of ready product (Jia et al., 2019). Optimisation of the drying process is therefore a topic of considerable interest from both economic and environmental standpoints. Based on a feasibility evaluation of wood dryers Lamrani et al. (2021) recommended waste heat recuperation.

To be able to control a process, the process mechanisms have to be adequately described and measures identified for determination of the optimal conditions of the process. Mathematical models based on energy and mass balances are capable of describing drying processes including convective dryers, see, for example, (Gaillemard, 2006; Smit et al., 2007; Thant et al., 2009; Rouch, 2010; Laurijssen et al., 2010; Jamaleddine & Ray, 2010; Sandoval Torres et al., 2011; Baxi et al., 2015; Di Marco et al., 2016; Gluesenkamp et al., 2019). In particular, Euh et al.

(2018) developed a real-time drying control that was capable to improve the drying efficiency of a pneumatic conveying dryer. The veneer drying process is based on the physical principles of moist air thermodynamics and moisture mass transfer. Thus, the limiting factors of convective evaporation are air humidity, temperature and mass transfer rate of moisture from the veneer surface to the bulk of the air, as shown in Figure 1. Process intensification and apparatus performance optimisation consequently tend to focus on these areas.

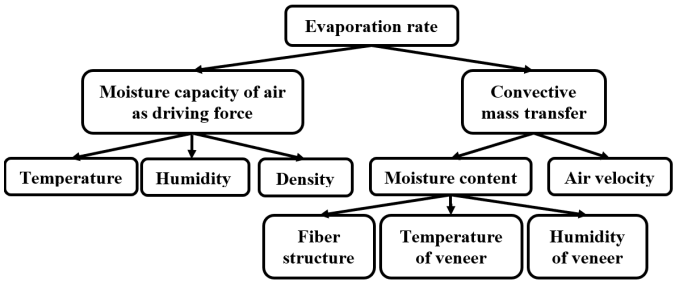

Figure 1: Diagram of evaporation rate.

In the published literature, there are examples of convective dryers modelled at different scales and using different approaches. Thant et al. (2009) proposed a simplified model for drying time estimation in a veneer jet dryer where internal and external moisture transport is considered. The model results agree with the experimental data reasonably well, however, the simulated time is quite short, during which the moisture transport to the veneer surface is intensive and doesn't limit the overall drying rate. The effect of air humidity and convective mass transfer was not considered. A CFD simulation was used by Rouch (2010) to estimate the airflow hydrodynamics and heat transfer in a wood plates drying. The wood plates package was considered as porous media and the drying rate was assumed constant. Regardless of missing validation, the modelling approach is robust and the results are adequate. In another work, Sandoval Torres et al. (2011) proposed a one-dimensional model for moisture transport through European oak and evaporation rate from the wood surface in a vacuum chamber. Wood layer was considered as porous medium. Assuming homogeneous air conditions in the vacuum chamber, the moisture transport due to convection was disregarded. Semi-empirical models of a rotary dryer and a textile dryer were developed in MATLAB Simulink by Baxi et al. (2015). Based on mass and energy balances, both models included the effect of air convection, material residence time and convective heat transfer. The model performance appeared adequate, however, a validation is missing. Di Marco et al. (2016) made a mathematical model for an air impingement dryer to evaluate the energy performance. The model prediction was within 5% deviation from experimental data with the assumption of constant humidity and temperature profiles in the dried tissue. It should be noted that thus far detailed dynamic models, describing a complex performance of a continuous convective drying unit, including humidity control mechanisms, have not been presented.

Experimental work, modelling and simulation are the three main approaches used in process engineering to understand phenomena such as drying (Zhang et al., 2020). A multi-parameter model of a complex process requires performance evaluation using varying input parameters to foresee different scenarios of the modelled process outcomes as illustrated in Figure 2. A comparative study of uncertainty quantification methods by Cox & Baybutt (1981) shows that the research on uncertainty quantification in models of physical processes dates as far back as 1981 (Zhang et al., 2020). Sensitivity analysis methods applied in different areas have been discussed in many studies, for example, (Kleijnen, 1995; Cacuci, 2003; Kleijnen, 2005; Bose et al., 2006; Saltelli et al., 2008; Lin et al., 2012; Kalyanaraman et al., 2015; Borgonovo & Plischke, 2016; Burnaev et al., 2017; Bhattacharyya, 2018).

Saltelli et al. (2008) discussed the principles and methods of sensitivity analysis with succinct definition of sensitivity analysis as the study of how variation in output of a model is explained by variation in the model inputs. The classical methods of sensitivity analysis and their corresponding problems cases have been discussed in the works of (Saltelli et al., 2008; Cacuci, 2003; Borgonovo & Plischke, 2016; Woods & Lewis, 2017). Sensitivity analysis methods varies from the historical approach of local sensitivity analysis where effects of local input perturbations on the model output is studied; design of experiment theory; Monte Carlo techniques and global sensitivity analysis that don't restrict the domain of model inputs (Saltelli et al., 2008).

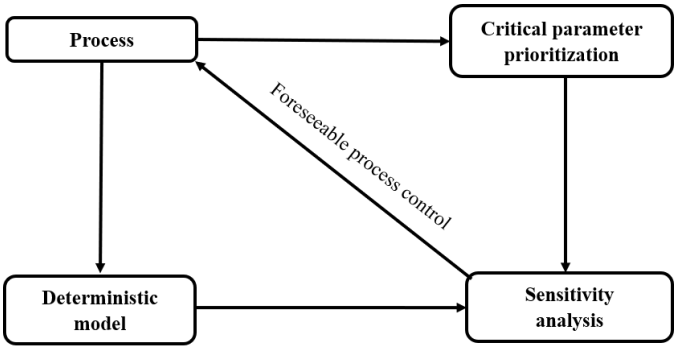

Figure 2: Process performance predictability analysis of mechanistic model.

Sałat et al. (2017) used a black-box approach to optimise the fan speed in an industrial-scale convective dryer. Bose et al. (2006) examined an uncertainty analysis of laminar aeroheating predictions for Mars entries. A Monte Carlo sensitivity and uncertainty analyses were used by (Bose et al., 2006) to investigate the effect of some selected parameters under Mars entry conditions of the model. The results gave a quantitative explanation of the uncertainties in the modelling parameters. Specifically, the collision integral in high and low catalytic regimes responsible for transport properties of mixtures contributes largely to the uncertainty.

Woods & Lewis (2017) reviewed methods from design of experiments developed from both physical experiments and those

related to numerical models. The classes of factorial designs were used to investigate main effects and interactions in the model with the active input variables providing information for optimisation of the model output.

The aim of this work is to create a dynamic model describing the convective drying process of veneer in a continuous drying unit. The model comprises energy and mass balances of moving air and veneer passing through the dryer. The model is then used to analyse the variation of the crucial parameters within the expected range, defined based on the performance practice of the drying unit. This paper covers the principles of modelling for the convective drying in Section 2. Section 3 describes the implementation of the convective dryer model in the environment of MATLAB Simulink. The results from the model simulations and sensitivity analysis are presented in Section 5.

2. Principles and modelling concepts of convective drying

The thermodynamics of the convective drying process is derived from the ideal gas law. Dry air and water vapour coexist in a domain under ambient pressure which is the sum of their partial pressures:

$$p^{\text{air}} + p^{\text{H}_2\text{O}} = p^{\text{atm}}. \tag{1}$$

Water molecules can diffuse from surface to air. Equilibrium moisture concentration in air is limited by the saturation pressure in the atmosphere (atm):

$$p_{\text{sat}}^{\text{H}_2\text{O}} = \exp\left(\frac{A}{T} + B + CT + DT^2 + ET^3 + G\ln T\right), \tag{2}$$

where T is the temperature of the air, $A{-}G$ and K, are the empirical constants (Steven et al., 2004). An increase in temperature leads to exponential growth of the saturation concentration of the water vapour. The molar flux of moisture from veneer plate to air can be expressed as follows:

$$M^{\text{H}_2\text{O}} = A_{\text{v}} k_{\text{g}} (p_{sat}^{\text{H}_2\text{O}} - p^{\text{H}_2\text{O}}), \tag{3}$$

where A_{v} is the contact area of veneer, m^2; k_{g} is the convective mass transfer coefficient, m/s (Welty et al., 2020). Molar flux conversion into mass flux results in the following expression:

$$\dot{m}^{\text{H}_2\text{O}} = A_{\text{v}} M^{\text{H}_2\text{O}} k_{\text{g}} (c_{\text{sat}}^{\text{H}_2\text{O}} - c^{\text{H}_2\text{O}}), \tag{4}$$

where M^{H_2O} is the molar mass of water, $kg/kmol$; c is the concentration of air water vapour, $kmol/m^3$. The convective mass transfer coefficient describes the transport efficiency of the moisture from the surface to the air bulk. It depends on airflow velocity at surface and water molecules diffusion. The convective mass transfer from a flat plate can be correlated with Reynolds ($\frac{\text{convection}}{\text{viscosity}}$) and Schmidt ($\frac{\text{viscosity}}{\text{diffusion of species}}$) dimensionless numbers as follows:

$$k_{\text{g}} = ARe^{1/2} S c^{1/3}, \tag{5}$$

where A is the empirical constant, 0.332 and 0.664 for laminar and turbulent regimes respectively (Welty et al., 2020).

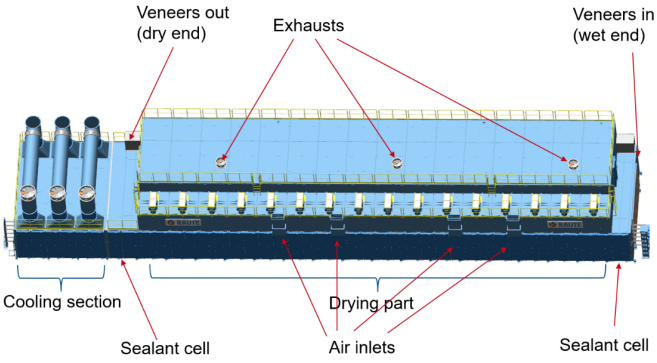

Figure 3: Illustration of the veneer dryer unit.

The drying unit, shown in Figure 3, consists of a drying section, comprising 16 drying cells, 2 smoke or sealant cells adjacent to the outer cells of the drying section, and 3 sequential cells of cooling section. The convective evaporation takes place in the drying cells, where blown air, heated by a radiator, streams continuously across the veneer sheets. The outer drying cells of the drying section are connected to the sealants or smoke cells. Leaving the second smoke cell, the veneer plates pass through the cooling section for temperature conditioning before they can be man handled. The hot fluid used in the radiators can be optionally steam or oil. A typical drying cell comprises a fan, a radiator, jet boxes, rollers, and optional air inlet and/or outlet, as shown in Figure 4.

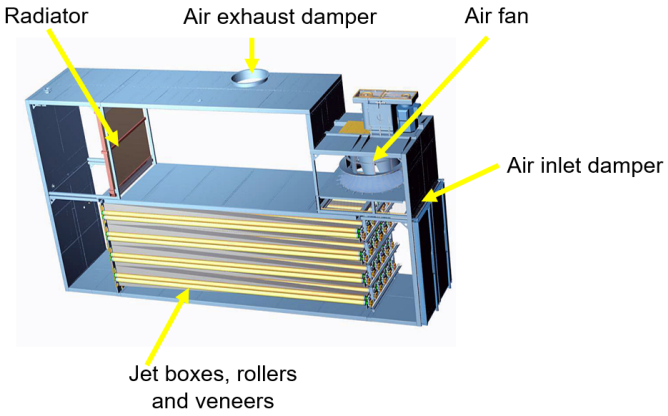

Figure 4: Illustration of the main features in the drying cell.

The geometry of the surface and the surrounding structures affects the mass transfer coefficient greatly. For simplified cases of flat or cylindrical surfaces in open space, the constants are sufficiently accurate. With complicated structures, however, such as the perforated jet boxes in the dryer in Figure 5, computational fluid dynamics (CFD) analysis can provide more accurate values (Jamaleddine & Ray, 2010).

Elevated temperature of the air increases the saturation concentration promoting higher drying rate. The diffusion of moisture through the veneer layers lowers the overall drying rate. In

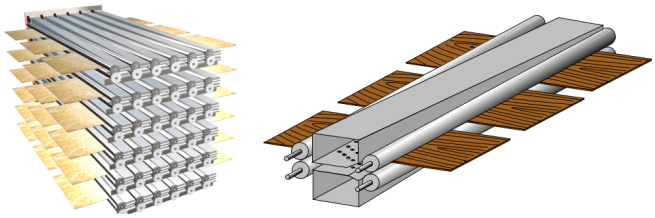

Figure 5: Illustration of the rollers on the left and jet boxes on the right.

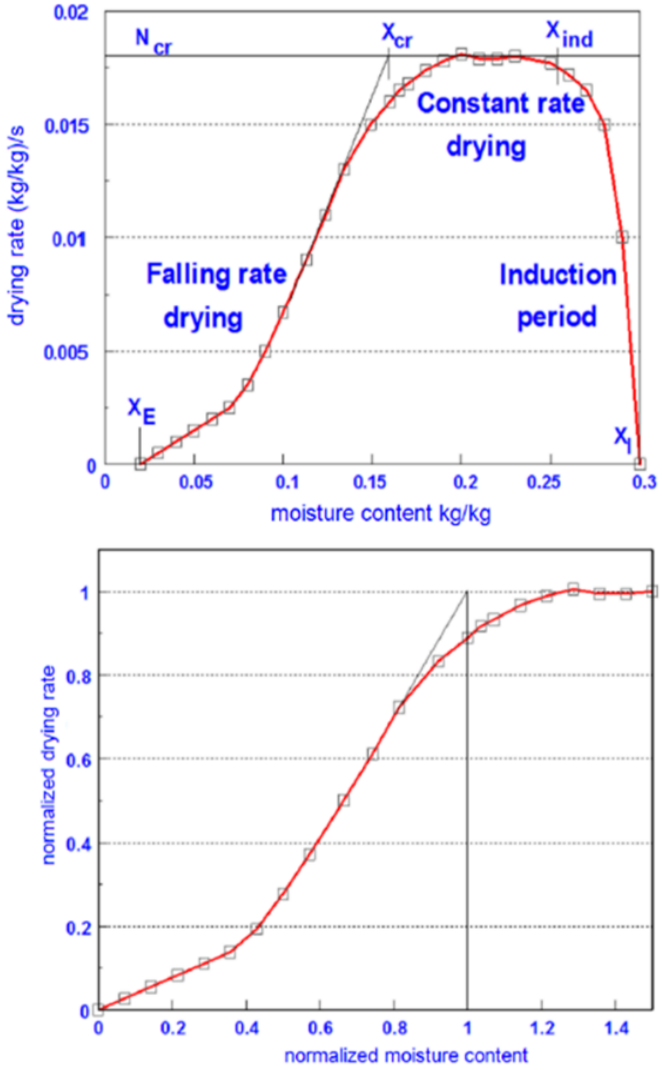

Figure 6: Normalisation of typical empirical drying rates as a function of moisture on the left and normalised quantities on the right (Lakshmanan & Claus, 2013).

practice, the diffusion time scale is small as the veneer sheets are thin and the moisture migrates from the middle of the sheets in both directions towards surface. Temperature affects moisture diffusion in fibres which can be described by Fickian Law or empirically. When a moist veneer plate enters the first drying chamber the moisture transport is increased due to convective heating during the induction period until a constant drying rate is reached. A constant drying rate is maintained until the veneer humidity reaches a critical value, whereupon the diffusion of the water becomes the limiting factor of the drying process, as illustrated in Figure 6. The reduction in the drying rate continues until an equilibrium moisture content is reached. The moisture driven limitation of the constant drying rate can be measured experimentally in similar conditions. The measured isotherm of the falling rate is normalised for modelling purposes. The empirical approach is a consistent and a simpler alternative to a detailed CFD model of the moisture transport through the material. Normalization procedure according to Equations 6 and 7 of the experimental data is shown in Figure 6 (Mujumdar, 2014).

$$\dot{m}_{\text{evap}}^{\text{norm}} = \frac{\dot{m}_{\text{evap}}^{\text{i}}}{\dot{m}_{\text{evap}}^{\text{const}}}. \tag{6}$$

$$X^{\text{norm}} = \frac{X_i - X_{\text{eq}}}{X_{\text{cr}} - X_{\text{eq}}}. \tag{7}$$

$$X = \frac{m^{\text{H}_2\text{O}}}{m^{\text{dry veneer}}}, \tag{8}$$

where X is the moisture content of the dried veneer.

2.1. *Design and functionalities of the drying cell*

Drying cell is a functional unit in the veneer dryer, hence a single cell can be modelled and then combined in a battery of 16 units to make the model of the veneer drying part. The modelled drying cell was divided into four sub-blocks of different functionality following the design presented in Figure 7 where air is assumed to be completely mixed.

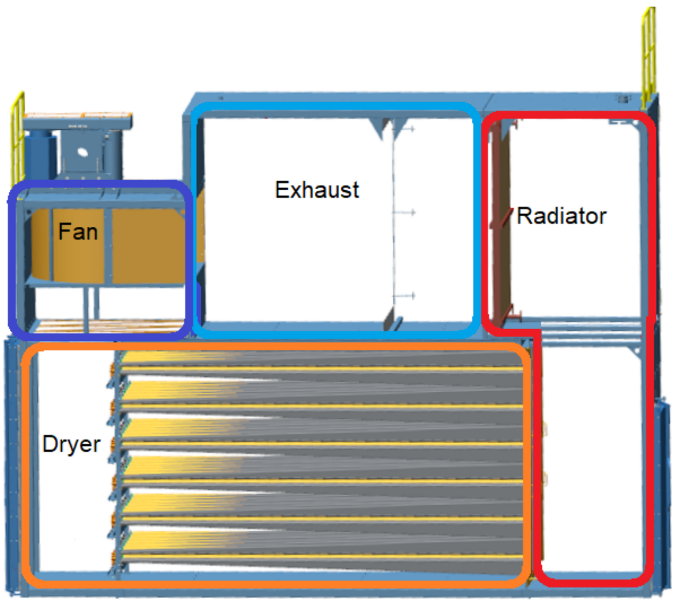

Figure 7: Illustration of the drying cell with conditionally outlined sub-blocks.

The starting point for the model design was the fan, which blows air towards the radiator. The sub-block, coloured in blue,

includes the inlet damper for two reasons. The first reason is the compactness of the model. The driving force for incoming fresh air is the negative pressure created by the fan. As an input parameter to the function for the mass flow rate, it is convenient to locate the static pressure at the damper and the fan in the same sub-block. The second reason is to exclude the heat impact of fresh air on the veneer drying process. The exhaust sub-block occupies the space from the fan sub-block to the radiator and by default includes an outlet, which can be optionally deactivated. The radiator sub-block starts from the radiator and occupies the vertical path of the air until the veneer transport structure. The remaining space is marked as a dryer sub-block and includes the material and energy balances of the air and veneer.

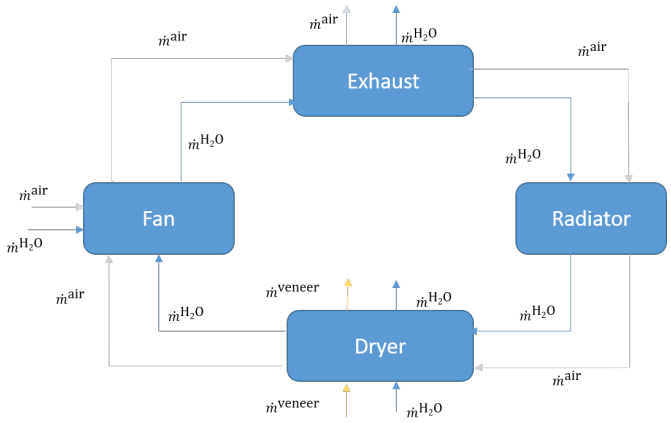

Figure 8: Mass balance diagram of the drying cell.

The mass balance in a typical drying cell is presented schematically in Figure 8, where the mass flow streams are shown. The material balance of air and water vapour has only one inlet and outlet that are in balance at the start but later can be changed dynamically by PID controllers. There is a source of water vapour evaporated from the veneer surface in the dryer sub-block. The released water reduces the veneer humidity via a sink term, which was added to the outlet mass flow rate in order to preserve the mass balance. Later, this artificial mechanism was removed until PID controllers and freely flowing air between cells were implemented.

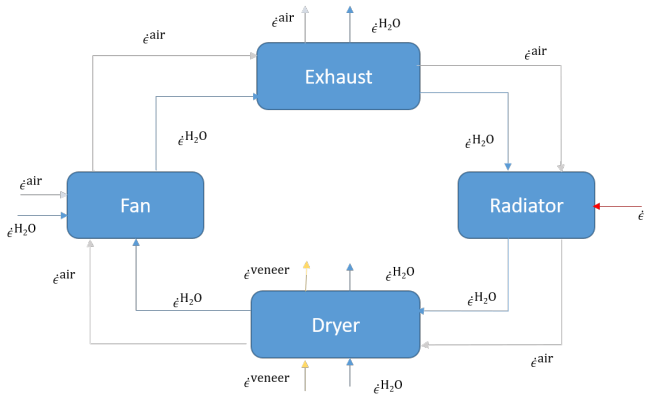

Figure 9: Energy balance diagram of the drying cell.

Energy balance in a typical drying cell is presented in Figure 9. Input fresh air reduces the energy and lowers the humidity. In the exhaust sub-block, the air loses energy through the air released to the outer environment. The radiator is the source of energy. The heat exchange and evaporation affect both the air and veneer energy streams. A detailed description of each sub-block is given in Section 3. The following features were implemented in the model: Mass and energy balances of air and veneer in the drying and smoke cells, a dynamic model of the radiator surface temperature, energy storage in the metal parts, the opening angle of the exhaust dampers is controlled by the PID controller, the opening angle of the inlet dampers is controlled by the PID controller, the recirculating gas moves between the cells based on static pressure, on/off switches for the inlet and outlet dampers, the properties of the air and veneer are adjustable, and the veneer transport speed and loading regime are adjustable.

3. Modelling continuous drying unit with MATLAB Simulink

The Simulink model was designed with the following assumptions and simplifications: the model excludes minor factors of influence; the fan maintains a constant volumetric flow rate; the heating agent has constant temperature; the air stream is assumed as perfectly mixed flow within sub-blocks; no temperature gradient profiles are considered in the veneer plates and metal parts; no heat exchange with the outer atmosphere is modelled; the effect of veneer temperature on moisture diffusion is omitted; and fan sub-blocks are isolated from each other.

The modelling environment of MATLAB Simulink has block-based approach where the functional blocks that are explicitly connected with the signal routes. The overall view of the model built in Simulink follows the construction of the real dryer (see Figure 10). The constituent elements are shown in Figure 11.

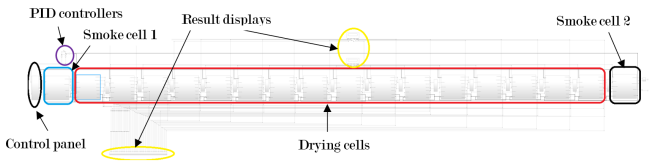

Figure 10: Architecture of the drying model in MATLAB Simulink.

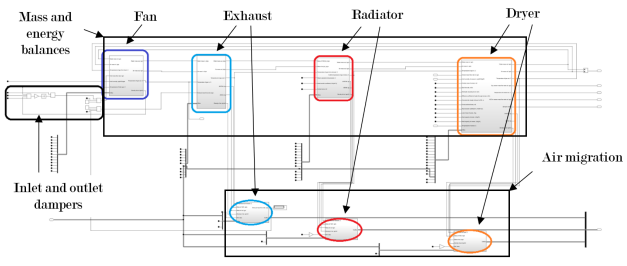

Figure 11: Architecture of the drying cell in MATLAB Simulink.

The exhaust, radiator and dryer sub-blocks have additional modules, calculating the static pressure and the flow rates of air migration between adjacent cells. The airflow rates through the dampers are calculated separately using the signals from the PIDs, the air properties in the outer area, in the fan and exhaust sub-blocks.

The mass and energy balances in fan sub-block are identical having two source and one sink terms. The fresh air source term is the function of the negative static pressure created by the fan and the damper lid angle. The exhaust sub-block has a large adjacent area between drying cells. Pressure driven airflow between neighbouring cells was therefore implemented. It is described in Section 3.2. The outlet damper releases the moist air based on the static pressure. The balances are identical having two sink and one source term. The sink term is a function of the static pressure created by the fan at the damper lid and the angle of the position of the damper lid automatically driven by the PID controller. The radiator sub-block has a large adjacent area with a neighbouring drying cell. Airflow between neighbouring cells was therefore implemented. The energy balance has an extra source term of the radiator, which supplies energy via a convective heat transfer mechanism from the hot surface temperature of the radiator to the gas mixture. The mechanism of the heat exchange between the heating fluid (steam) and the radiator surface is implemented in the model. It is described in Section 3.3. The pressure drop of the gas passing through the radiator is significant. The geometric configuration of the radiator as well as the number of radiating plates affect the pressure drop.

The dryer sub-block has a large adjacent area between drying cells. Airflow through the adjacent area between neighbouring cells was therefore implemented. The static pressure of the hot gas passing through the jet box comprises less than 5% of the initial static pressure at fan, which was measured in an actual dryer on site.

The principle equations upon which the sub-blocks were built are listed below:

$$\dot{m}_{\mathrm{acc}} = \dot{m}_{\mathrm{in}} - \dot{m}_{\mathrm{out}}. \tag{9}$$

$$\rho^{\mathrm{mix}} = \frac{m^{\mathrm{H_2O}} + m^{\mathrm{air}}}{V}. \tag{10}$$

$$f^{\mathrm{H_2O}} = \frac{m^{\mathrm{H_2O}}}{m^{\mathrm{H_2O}} + m^{\mathrm{air}}}. \tag{11}$$

$$\dot{m}^{\mathrm{mix}}_{\mathrm{out}} = \dot{q}_{\mathrm{fan}} \rho^{\mathrm{mix}}_{\mathrm{fan}}. \tag{12}$$

$$\dot{m}^{\mathrm{mix}}_{\mathrm{damper}} = A_{\mathrm{lid}} \left(2\rho_{\mathrm{mix}} P^{\mathrm{mix}}_{\mathrm{st}}\right)^{1/2}. \tag{13}$$

$$P^{\mathrm{mix}}_{\mathrm{st-ex}} = P^{\mathrm{mix}}_{\mathrm{st}}(T_{ref}) \frac{\rho_{\mathrm{mix}}(T) T}{\rho_{\mathrm{mix}}(T_{ref})}. \tag{14}$$

$$P_{\mathrm{st-rad}} = C^{\mathrm{rad}}_{\mathrm{f}} P^{\mathrm{mix}}_{\mathrm{st-ex}}. \tag{15}$$

$$P_{\mathrm{st-dry}} = C^{\mathrm{dryer}}_{\mathrm{f}} P^{\mathrm{mix}}_{\mathrm{st-ex}}. \tag{16}$$

$$\dot{m}^{\mathrm{H_2O}}_{\mathrm{veneer\_air}} = A_{\mathrm{veneer}} f_{\mathrm{evap}} k_{\mathrm{g}} (c^{\mathrm{H_2O}}_{\mathrm{sat}} - c^{\mathrm{H_2O}}) M_{\mathrm{H_2O}}. \tag{17}$$

$$\dot{\epsilon}_{acc} = \dot{\epsilon}_{in} - \dot{\epsilon}_{out} - f^{H_2O} \dot{\epsilon}_{\mathrm{heat}}. \tag{18}$$

$$\dot{\epsilon} = \dot{m} h = \dot{m} c_{\mathrm{p}} T. \tag{19}$$

$$\dot{\epsilon}_{\mathrm{evap}} = \dot{m}^{\mathrm{H_2O}}_{\mathrm{veneer\_air}} \lambda_{\mathrm{H_2O}}. \tag{20}$$

$$\dot{\epsilon}_{\mathrm{rad}} = U_{\mathrm{rad}} A_{\mathrm{rad}} (T_{\mathrm{rad}} - T^{\mathrm{mix}}_{\mathrm{in(exhaust)}}). \tag{21}$$

$$\dot{\epsilon}_{\mathrm{heat}} = U_{\mathrm{veneer}} A_{\mathrm{veneer}} (T^{\mathrm{mix}}_{\mathrm{in(exhaust)}} - T^{veneer}_{\mathrm{in}}). \tag{22}$$

$$T_{\mathrm{rad}} = \frac{U_{\mathrm{rad}} A_{\mathrm{rad}} (T_{\mathrm{steam}} - T_{\mathrm{rad}})}{m_{\mathrm{rad}} c^{\mathrm{metal}}_{\mathrm{p}}}. \tag{23}$$

$$T^{\mathrm{mix}}_{\mathrm{out}} = \frac{\dot{\epsilon}^{\mathrm{mix}}_{\mathrm{acc}}}{\dot{m}^{\mathrm{H_2O}}_{\mathrm{acc}} c^{\mathrm{H_2O}}_{\mathrm{p}} + \dot{m}^{\mathrm{air}}_{\mathrm{acc}} c^{\mathrm{air}}_{\mathrm{p}}}. \tag{24}$$

The moisture and dry air mass balance in the sub-block are described in Equation 9, where $\dot{m}_{\mathrm{acc}}$ is the mass accumulated in the sub-block, and $\dot{m}_{\mathrm{in}}$ and $\dot{m}_{\mathrm{out}}$ are mass inflows and outflows respectively. The density of gas mixture in Equation 10 denoted by ρ^{mix} is the ratio the mixed masses (moisture mass $m^{\mathrm{H_2O}}$ and air mass m^{air}) and the sub-block volume V. The water vapour mass fraction in Equation 11 denoted by $f^{\mathrm{H_2O}}$ is the ratio of the water mass and the mixed masses. The static pressures in the exhaust, radiator and dryer sub-blocks depend on pressure loss in the corresponding sub-block ($C^{\mathrm{i}}_{\mathrm{f}}$) due to airflow channel construction as described in Equation 14 - 16. The sink term of mass flow rate $\dot{m}^{\mathrm{mix}}_{\mathrm{out}}$ is described in Equation 12, mass flow rate through dampers $\dot{m}^{\mathrm{mix}}_{\mathrm{damper}}$ is described in Equation 13, evaporation rate in veneer $\dot{m}^{\mathrm{H_2O}}_{\mathrm{veneer\_air}}$ is described in Equation 17, energy rate $\dot{\epsilon}$ is described in Equation 19, the energy transfer rate due to evaporation $\dot{\epsilon}_{\mathrm{evap}}$ is described in Equation 20, heat duty of radiator sub-block $\dot{\epsilon}_{\mathrm{rad}}$ is described in Equation 21, air-veneer heat transfer rate $\dot{\epsilon}_{\mathrm{heat}}$ is described in Equation 22, radiator temperature T_{rad} is described in Equation 23, temperature of leaving gas mixture $T^{\mathrm{mix}}_{\mathrm{out}}$ is described in Equation 24. c_{p} is the specific heat capacity of a phase, U is the heat transfer coefficient, h is the enthalpy, λ is the latent heat. The phase components such as moisture (H_2O), dry air (air), and gas moist air (mix) are denoted as symbols superscripts, while the drying unit parts and flow directions are specified as symbol subscripts in the equations.

The experimental reference data was provided by Raute Oyj (Figure 12).

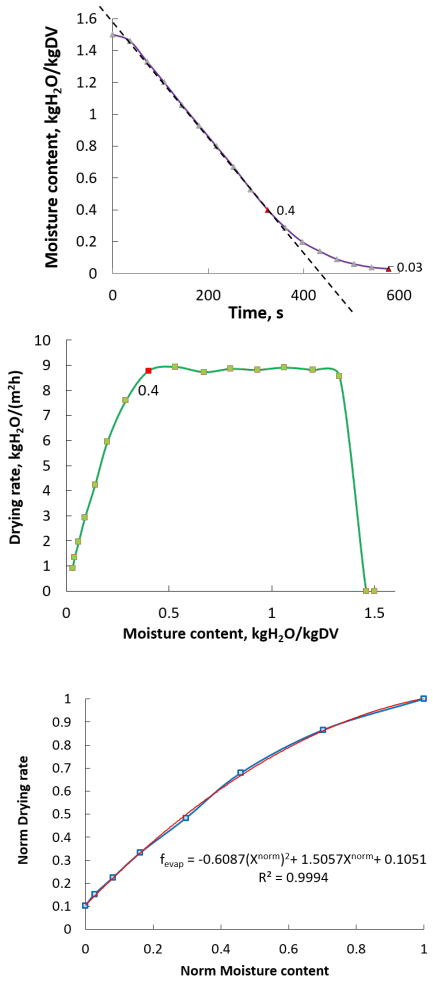

Figure 12: Measured drying rate of veneer plate at 63C (upper), derived drying isotherm (middle) and normalised drying isotherm (lower). The blue line shows the curve while red line is polynomial trend line.

The falling period of the normalised drying rate isotherm was fitted using the polynomial presented in Figure 12. Similarly, the induction drying rate period can be modelled when the necessary data is provided as mentioned in Section 2, however, the temperature-induced moisture diffusion through the veneer thickness is to be determined.

To obtain the convective mass transfer coefficient, three different methods were tested. Following the complexity growth of the methods, the first method was using a direct empirical value, which was taken as the most reliable number and set as a default. However, the flow rate at the fan affects the Schmidt and Reynolds numbers, therefore two other methods were implemented, namely: fully mechanistic formulations for the both dimensionless numbers and semi-empirical where an empirical value for the Reynolds number was used.

3.1. Airflow between adjacent sub-blocks of neighbouring cells

The mechanism of air transport from cell to cell is based on the static pressure at adjacent areas of parallel air flows where they interact. The pressure is linearly dependent upon the gas mixture density and temperature, as presented in Equation 14. Based on the pressure difference between adjacent sub-blocks of neighbouring cells, the mass flow rate can be found in a similar way to the mass flow rate through the damper in Equation 13. The sign of the pressure difference defines the direction of the flow. It must be noted that the corresponding density and temperature of the dominating airflow are to be used to preserve the mass and energy balances.

A different situation is found with smoke cells that don't have a fan but contact with a dryer sub-block in the outer drying cells. These cells are preheated with hot air coming from the radiator sub-block domain through a small "window". The reference static pressure approach in Equation 14 works fine to find the pressure difference between drying cells, but it is very inaccurate when a pressure value is used against the absolute pressure in the smoke cells, and it produces unrealistically high values of driving pressure. Therefore, in the outer drying cells, as well as the reference static pressure, the absolute pressure is also calculated, which is used to obtain the mass flow rate between the dryer sub-block and smoke cell. The other side of the smoke cell is connected to the outer atmosphere or the cooling section, which is assumed to have atmospheric conditions. The air mass flow rate is simulated based on the difference in absolute pressures. As the transported veneer is in contact with the air in the smoke cells, the heat exchange mechanism is implemented and evaporation is omitted.

3.2. Energy accumulation in metal parts

Metal parts such as fans, radiators, dryer walls, jet boxes, and rollers have significant mass that can accumulate and release energy. The corresponding energy balances including the heat transfer between the gas and metals were implemented in every sub-block. During heating up, the metal parts strip energy from the passing air, which slows down the cooling process in the case of a sudden shutdown of the dryer.

3.3. Inlet and outlet dampers with PID controllers

PID controllers manage the position of the damper lids. The controllers use static pressure readings in the smoke cells as target parameters. Based on the conventional performance of the dryer, mild pressure (5-10 Pa) should be maintained to ensure fresh air is fed into the dryer from both ends. The free parameter of the PID controller, $k^{-(1/2)}$, is controls the angle of the position of the damper lid that enhances or limits the airflow rate of Equation 27: 25

$$\dot{m}^{\mathrm{mix}}_{\mathrm{damper}} = A_{\mathrm{lid}} \left(\frac{2\rho_{\mathrm{mix}} P^{\mathrm{mix}}_{\mathrm{st}}}{k} \right)^{1/2} . \tag{25}$$

The PID controllers are limited by a range of $k^{-(1/2)}$ to avoid the risk of the unrealistic values. In the current model, the free parameter is limited between 0.025 and 35 according to the empirical data provided by the manufacturing company Raute Oyj.

4. Methodological framework for sensitivity analysis

Simulations in sensitivity analysis are conducted to account for the variation in the model output due to variation in the input (Zhang et al., 2020). The spread realised from using different initial values of the model are evaluated and analysed. This method can be represented as:

$$\mathbf{y} = \mathcal{H}(\mathbf{x}), \tag{26}$$

where $\mathcal{H}$ is a vessel function and in this case a deterministic Simulink model with input parameters of the model $\mathbf{x}$ constituting the feature space and an output vector $\mathbf{y}$ representing the final veneer humidity and power consumption throughout the drying process.

4.1. Factorial experimental design for continuous veneer unit model

A systematic approach to experimental design eliminates researcher bias and reveal the interaction of the input signals and its effect onto the response variable (Steven et al., 2004). Widely used experimental designs in both research and industrial setting are the full and fractional factorial designs (Antony, 2014; Politis et al., 2017; Dante et al., 2003). The full factorial design requires L^k experiments, where L is the number of levels and k is the number of parameters in the experiment (Dante et al., 2003). The use of a design matrix is to replace the ideal case of operational data as input to the model. The full factorial design gives a parsimonious modelling by constraining the parameters to all the discrete possible combinations of the levels across the factors (Antony, 2014). The dimension of the feature space is a $p \times k$ matrix and the output from the model is a $n \times p$ matrix. This implies k parameters are to be varied for $p = L^k$ iterations and n is the model simulation time.

The parameters varied in the simulation were veneer initial, veneer humidity, radiator temperature, atmospheric pressure, conveyor belt speed, and volumetric flow rate of fan. The degree of variance for each parameter is subjective and it was chosen based on the practice of the drying unit operation in South Karelia region of Finland. The design matrix was converted from coded values to real values and used as model inputs, hence representing a 3^5 full factorial experiment.

4.2. Statistical framework for Analysis of Variance (ANOVA)

Statistical methods are used for explaining the relationship between the design response and the predictors (Hoaglin & Welsch, 1978; Faraway, 2002). ANOVA is used when predictors are fixed in advance or sampled together with the responses. The standard multiple linear regression model is of the form:

$$y = X\beta + \epsilon, \tag{27}$$

where y is the response vector, X is the design matrix, β is the co-efficient vector and ϵ is the error vector or residuals. The predicted value of the response is hence given by:

$$\hat{y} = X\hat{\beta} = X(X^TX)^{-1}X^Ty = Hy, \tag{28}$$

where $H = X(X^TX)^{-1}X^Ty$ is the hat matrix and $\hat{\beta} = (X^TX)^{-1}X^Ty$ is the least square estimate of β.

Table 2 is populated with the statistics from the regression model and residuals.

The sum of squares in the ANOVA table are calculated as follows:

$$\mathrm{SS}_{\mathrm{Reg}} = \sum (y_i - \bar{y})^2. \tag{29}$$

$$\mathrm{SS}_{\mathrm{Res}} = \sum (y_i - \hat{y}_i)^2 = (y - X\hat{\beta})^T(y - X\hat{\beta}) = \hat{\epsilon}^T\hat{\epsilon}. \tag{30}$$

$$\mathrm{SS}_{\mathrm{Total}} = \sum (y_i - \bar{y})^2 = (y - \bar{y})^T(y - \bar{y}). \tag{31}$$

For an experiment of k predictors and N observations, the regression model degrees of freedom (DF) is k, the residual degrees of freedom is $(N-k-1)$, and the total degrees of freedom is $(N-1)$. The mean square is the ratio of the sum of squares and their respective degrees of freedom.

4.3. Multi-objective Optimisation

Multi-objective optimisation techniques are useful in optimising problems with two or more often conflicting objective functions simultaneously. The application areas of multi-objective optimisation have triggered continuous research in meta-heuristic and multi-evolutionary optimisation techniques (Ehrgott, 2008; Jaimes et al., 2009; Coello, 2018).

The goal attainment method described by Gembicki & Haimes (1975) is widely used among the several techniques in multi-objective optimisation. The method involves a set of objective functions $F(x) = \{f_i(x)\}$, a set of corresponding goals to be attain for each objective function $F^*(x) = \{f_i^*(x)\}$, and weights $\omega = \{\omega_i\}$ that enable the under or over-achievement of the targets. The optimisation problem is hence constructed as

$$\begin{aligned} &\text{minimize} \;\; \gamma, \\ &\text{subject to} : f_i(x) - \omega_i\gamma \leq f_i^*(x), \\ &\qquad x \in X, \gamma \in \mathbb{R}, \end{aligned}$$

where γ is the attainment factor and X is the parameter domain of interest.

The two model outputs, final veneer humidity and total power consumption are optimised with the goal attainment method.

Control parameter	Low	Medium	High
Initial veneer humidity (IVH) ($kgH_2O/kgDV$)	1.0	1.5	2.0
Radiator temperature (RT) (°C)	165	205	245
Atmospheric pressure (AP) (Pa)	97300	101300	105300
Flow rate at fan (FR) (m^3/s)	15	25	35
Conveyor belt speed (CS) (m/s)	0.045	0.055	0.065

Table 1: Variation of control parameters used in the sensitivity analysis

Source	Sum of Sq.	DF	Mean Sq.	F-statistic
Regression	SS_{Reg}	k	SS_{Reg}/k	MS_{Reg}/MS_{Res}
Residual	SS_{Res}	$N-k-1$	$SS_{Res}/(N-k-1)$	
Total	SS_{Total}	$N-1$		

Table 2: ANOVA table statistics for regression model and residuals.

The regression models from the ANOVA results are used as the objective function. Henc, the problem is reduced to a two-objective optimisation problem:

$$\begin{aligned} &\text{minimize } \gamma, \\ &\text{subject to : } f_1(x) - \omega_1\gamma \le f_1^*(x), \\ &\qquad f_2(x) - \omega_2\gamma \le f_2^*(x), \\ &\qquad x \in X, \gamma \in \mathbb{R}. \end{aligned}$$

The weights ω_i are chosen such that $\sum_{i=1}^{2} \omega_i = 1$.

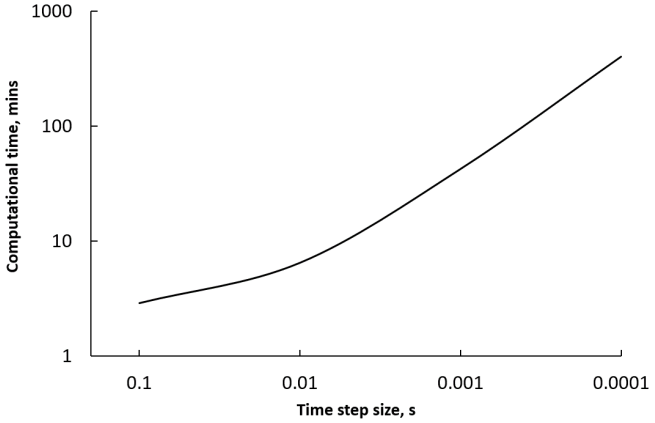

Figure 13: Calculation time of 1 hour simulation VS time step size at 8 CPUs i7-7000 and 32 Gb RAM.

5. Results and discussions

The performance of the simulator was evaluated in various work regimes, the results of which are presented in this section. First, the most simplified simulation without air flowing freely between cells was tested to limit the number of factors affecting the overall performance of the drying chambers. In addition, all the inlet and outlet dampers operated without PID controllers (fixed free parameter). The second simulation included air transport between the drying chambers while the dampers worked as in the previous simulation case. In the last case, the dryer worked in fully operative mode with active dampers, as shown in Figure 2. Inlet dampers 4, 6, 10, 12 and outlet dampers 2, 8, 14 were On while others were Off. The simulation results achieved at different initial conditions are presented together for comparison purposes as presented in Table 3.

The model was simulated for 1800 seconds with the time step of 0.01 seconds. The simulation took 4.5 minutes, of which compilation and initialisation took 2.5 minutes, approximately 0.7 millisecond per time step, using 8 CPUs i7-7000 and 32 Gb of operative memory. This information allows planning the simulation time for the cases where other time step size is chosen, see, for example, 13. The maximum size of a single time step is limited by the residence time of air in the smallest sub-block, in this case 0.1 seconds. To obtain more accurate results, the time step size can be decreased to 0.001 seconds. The dryer performance from startup to steady-state operation was simulated using three sets or cases of operational conditions. The simulation results obtained at different initial conditions are presented in Table 3. Drying rate curves for various simulation scenarios are presented in Figure 14. The veneer enters a drying cell with the gas-veneer contact area zero at the start, i.e. the moment the veneer sheets enter the drying chamber, and this contact area grows as the veneer is transported through the cell. The dynamic movement of the transported veneer was modelled in the simulations, which resulted in inclined vertical lines for the drying curves. As soon as the veneer reaches the maximum contact area, other limiting factors start dominating, such as the bearing capacity of the moist air and the humidity of the veneer.

Cases	Drying chamber connection	PID controller parameter, $k^{-(1/2)}$	Active inlet dampers	Active outlet dampers
1	No	2	All	All
2	Yes	2	All	All
3	Yes	0.025 – 35	4, 6, 10, 12	2, 8, 14

Table 3: Operating conditions of the veneer dryer defined for simulation.

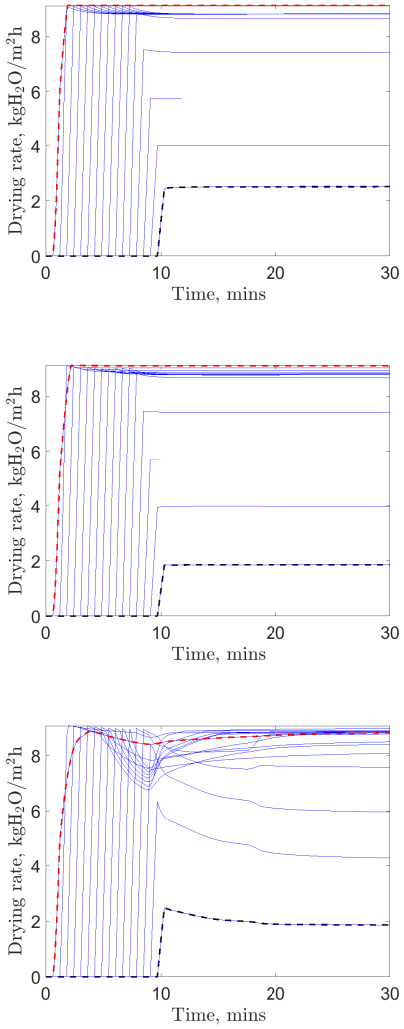

Figure 14: Simulation results for the drying rate in drying cells at three different simulation scenarios (cases 1-3). The drying rate of the first drying cell chamber is plotted with red dashes, the last chamber with black dashes and other chambers with blue lines.

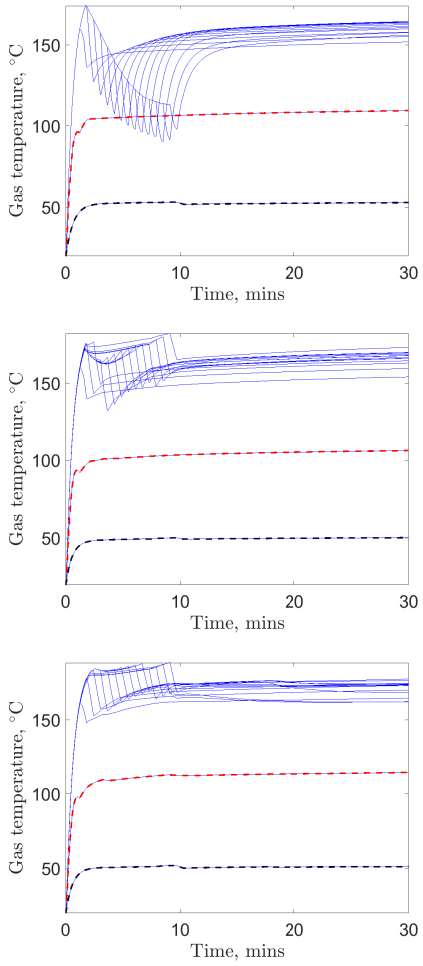

Figure 15: Simulation results for air temperature at the fan sub-block in the drying cells in three different simulation scenarios (cases 1-3). The air temperature in the first drying cell chamber is plotted with red dashes, the last chamber with black dashes and other chambers with blue lines.

Fully isolated drying cells have high air humidity, as seen in Figure 17, which limits the drying rate in all the cells (see Figure 14). The dynamic control of the dampers preserves the balance more efficiently. It can be used to minimise the heat duty of the radiators in the last five cells as the veneer approaches critical moisture content already in cell 12 of Figures 14 and 18.

Figure 15 presents the gas temperature at the fan sub-block. Pressure grows rapidly in an isolated cell as the temperature rises, pushing the outlet damper lid into the open position to let the air out. The outlet damper lid position affects the air humidity, which in turn influences the drying rate. The gas of reduced density carries less energy, which resulted in the temperature drop in case 1 of Figure 15 when veneer enters the cells. The freelly flowing air introduces more air into the cells. As can be seen in the figure, the outer drying cells 1 and 16 have lower air temperatures due to the connections with the smoke cells. The

optimised work of the dampers keeps the air humidity below 0.6 $kgH_2O/kgDA$. The reduced drying rate caused the smaller final veneer temperature in case 1 of Figure 16. The energy balance between convective heat transfer from gas to veneer and evaporation of water explains the plateau in the temperature of the veneer seen in cells 6 - 12.

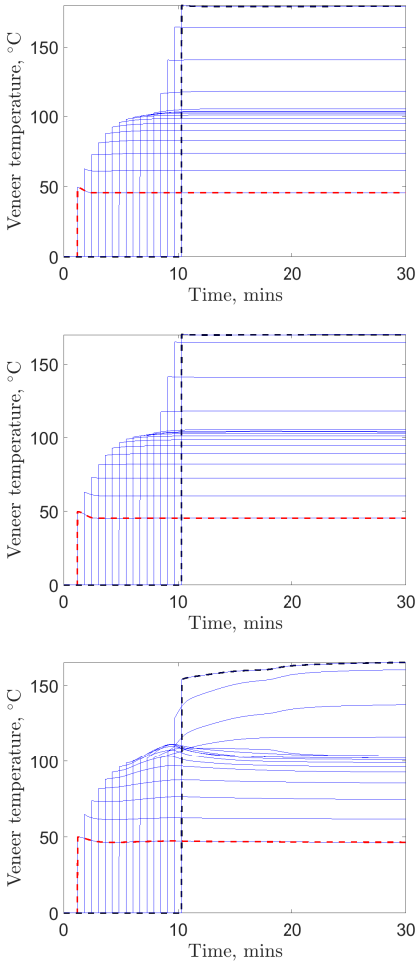

Figure 16: Simulation results for the temperature of the veneer exiting the drying cells in three different simulation scenarios (cases 1-3). The veneer temperature in the first drying cell chamber is plotted with red dashes, the last chamber with black dashes and other chambers with blue lines.

The moisture content of the veneer, shown in Figure 18 is best controlled in the interconnected drying cells using the PID controllers.

5.1. Sensitivity analysis results

The dryer model was used to simulate 30 minutes of drying performance. The control parameters were varied for the sensitivity analysis as described in Section 4.1. The simulated results of the final veneer humidity and the overall power consumption were stored for the ANOVA and optimisation of the parameters. The effect of the parameters was first examined graphically in

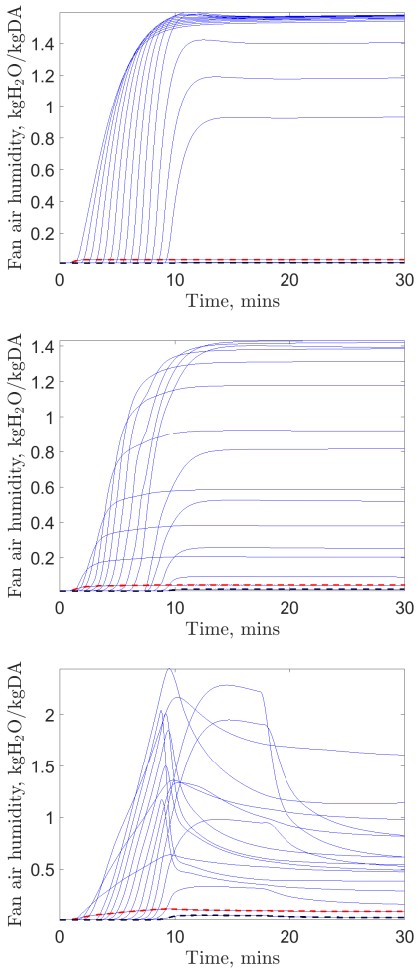

Figure 17: Simulation results for air humidity in the dryer sub-block in drying cells in three different simulation scenarios (cases 1-3). The drying rate of the first drying cell chamber is plotted with red dashes, the last chamber with black dashes and other chambers with blue lines.

Figure 19. It is clear that radiator temperature is the major factor increasing the drying rate as shown in Figure 19a. There is a slight relationship in term of the spread power consumption and initial veneer humidity in Figure 19b.

The regression results for the final veneer humidity in Table 4 show the coefficients of the control parameters and their interactions. The initial veneer humidity and interaction between the humidity and the radiator temperature have t-value significantly different from zero hence contributing meaningfully to the output. The ANOVA results in Table 5 also show that the regression model significantly explains the variation. Figure 20 presents the effect of radiator temperature and initial veneer humidity values on the final veneer humidity.

A similar analysis was implemented for the power consumption from the regression model of the response surface graphs. The results for the power consumption in Table 6 shows that the t-value of all parameters except conveyor speed are significant. The regression model doesn't consider the parameters interac-

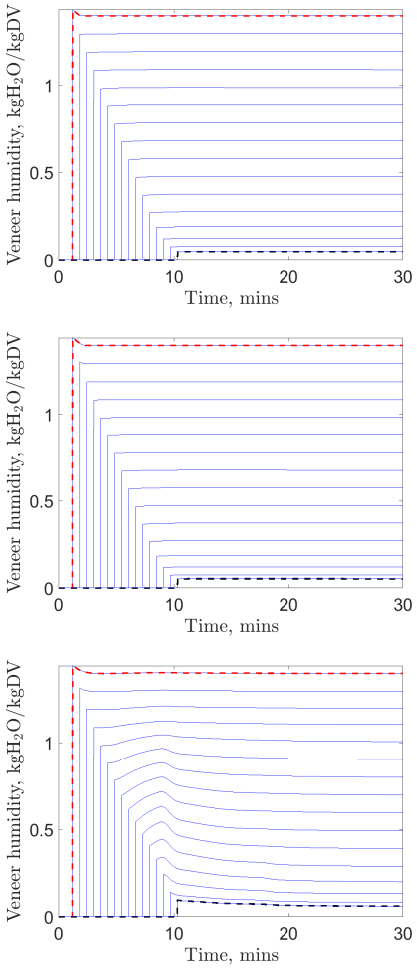

Figure 18: Simulation results for the moisture content of the veneer exiting the drying cells in three different simulation scenarios (cases 1-3). The veneer moisture content in the first drying cell chamber is plotted with red dashes, the last chamber with black dashes and other chambers with blue lines.

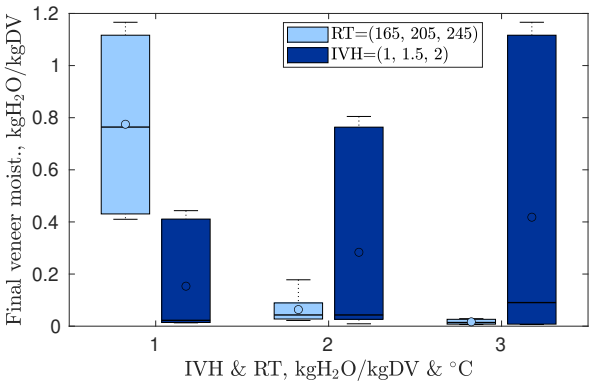

(a) Simulated final veneer humidity at different initial veneer humidity and radiator temperature.

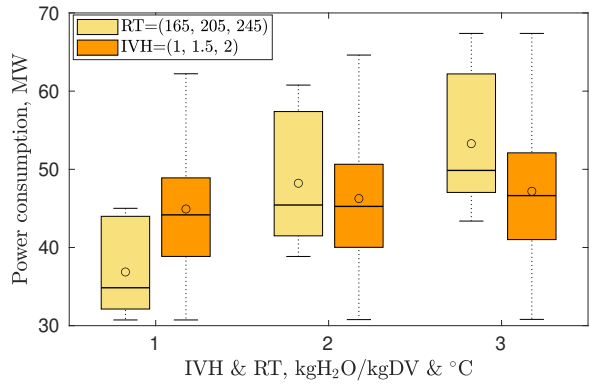

(b) Simulated power consumption at different initial veneer humidity and radiator temperature.

Figure 19: Design output of final veneer humidity and power consumption against radiator temperature and initial veneer humidity parameters.

tion as the linear model is parsimonious enough to describe the model and the variations in the model.

Figure 21 presents the effect of radiator temperature and initial veneer humidity values on the power consumption output. In an attempt to resolve the two conflicting objectives of minimising the final veneer humidity and power consumption, the goal attainment method of multiobjective optimisation is used. Hence, the objective functions are the regression models in Equations **??** and **??** characterising the final veneer humidity output and power consumption output with regards to the design parameters. The goals values for both outputs are 0.05 $kgH_2O/kgDV$ and 30.7 MW respectively. The domain of the input parameters was restricted to the design in Table 1. A multi-objective optimisation problem was constructed as explained in Section 4.3, thus, the optimal parameter values and the corresponding function output are presented in Table 8 and Figure 22.

The first set of the optimal values for both targets is 0.03 $kgH_2O/kgDV$ and 38.5 MW at initial veneer humidity of 1.5 $kgH_2O/kgDV$ and radiator temperature of 207.5°C. The second set is 0.06 $kgH_2O/kgDV$ and 37.1 MW at initial veneer humidity of 1.5 $kgH_2O/kgDV$ and radiator temperature of 205°C. At this point, an experienced decision marker is left to choose a desired solution from the available optimal values given.

6. Conclusions

Using the computational tools of MATLAB Simulink, a dynamic simulator for a continuous veneer dryer was built. The complicated mechanisms of heat and mass transfer inside the veneer dryer were described in a semi-empirical model. The model describes the convective mass transfer of moisture from veneer plates continuously transported through the dryer sections where the heated air is blown by fans cross-wise. In the model, a drying chamber is conditionally split into four sequentially connected sub-blocks, between which air can move. The system of damper lids operated by PID controllers is also modelled. The lids are opened more widely when the local air humidity rises. The moist air can move between the drying chambers towards the air outlet dampers driven by the static pressure.

Predictors	Coefficient	Standard Error	T-value	P-value
Intercept	0	6.432	0	1.000
IVH	1.970	0.326	6.052	0.000
FR	-0.009	0.016	-0.557	0.578
RT	-0.080	0.004	-18.48	0.000
CS	0	17.493	0	1.000
AP	$1.51 * 10^{-4}$	$1.257 * 10^{-4}$	1.2	0.231
IVH*ST	-0.009	$2.6 * 10^{-4}$	-33.87	0.000
ST^2	$2.1 * 10^{-4}$	$4.639 * 10^{-6}$	45.08	0.000

Table 4: Regression estimates of parameter coefficients and test of significance for the final veneer humidity model.

Source	Sum of Sq.	DF	Mean Sq.	F-statistic	P-value
Regression	35.317	20	1.766	593.51	0.000
Residual	0.661	222	0.003		
Total	35.978	242			

Table 5: ANOVA table statistics for regression model and residuals for final veneer humidity.

Predictors	Coefficient	Standard Error	T-value	P-value
Intercept	1.746	6.818	0.256	0.798
IVH	2.266	0.455	4.982	0.000
FR	-0.819	0.023	-36.03	0.000
RT	0.205	0.006	36.09	0.000
CS	5.751	22.739	0.253	0.801
AP	0.0002	$6.475 * 10^{-5}$	2.919	0.004

Table 6: Regression estimates of parameter coefficients and test of significance for power consumption model.

Source	Sum of Sq.	DF	Mean Sq.	F-statistic	P-value
Regression	22063	5	4412.6	526.77	0.000
Residual	1985.3	237	8.377		
Total	24048	242			

Table 7: ANOVA table statistics for regression model and residuals for power consumption.

IVH	FR	RT	CS	AP	Veneer humidity	Power consumption
1.5	35	207.6	0.045	101300	0.03	38.5
1.5	35	205	0.045	97300	0.06	37.1

Table 8: Optimal parameters values with corresponding target values of final veneer humidity and power consumption.

The installed sensors ensure a slight underpressure atmosphere in the smoke cells through the action of the PID controllers linked to the outlet dampers. The underpressure maintains the fresh air inflow from the premises outside the dryer. The transported veneer is heated while passing through the first seven cells until the maximum drying rate is reached. In the next five

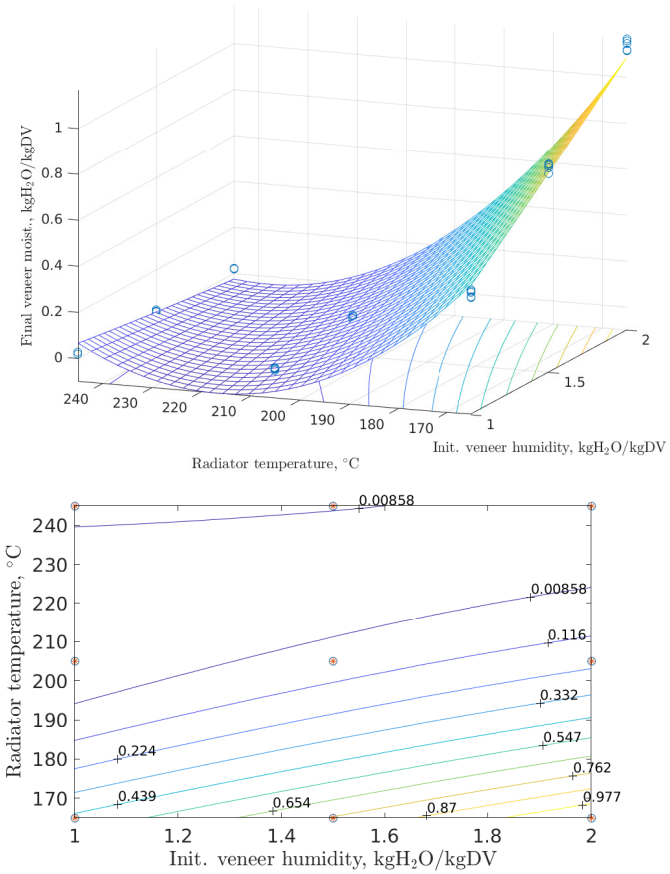

Figure 20: Radiator temperature and initial veneer humidity parameters effect on final veneer humidity at conveyor speed 0.045m/s, fan rate 35m^3/s and atmospheric pressure 1013hPa.

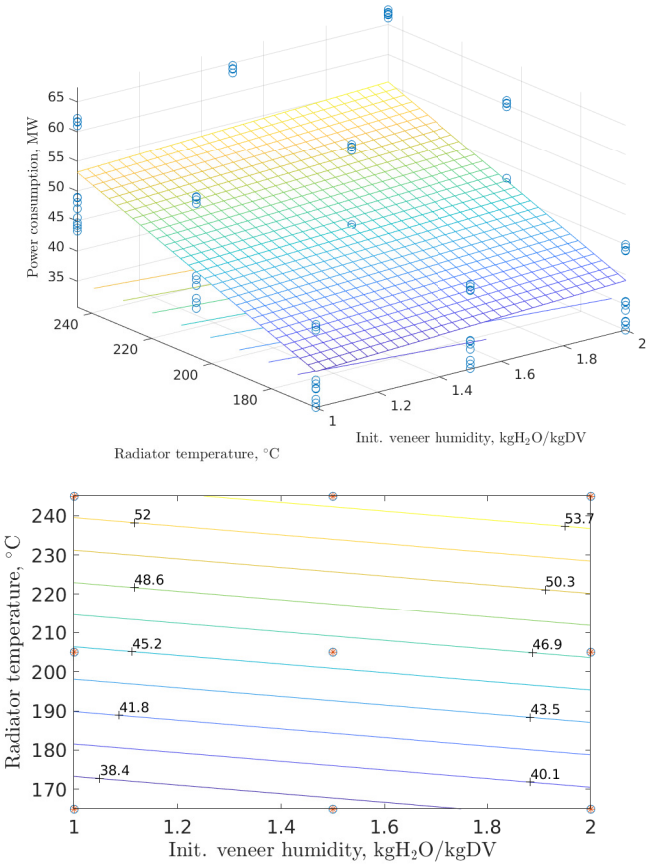

Figure 21: Radiator temperature and initial veneer humidity parameters effect on power consumption output with conveyor speed at 0.045m/s, fan rate at 35m^3/s and atmospheric pressure at 1013hPa.

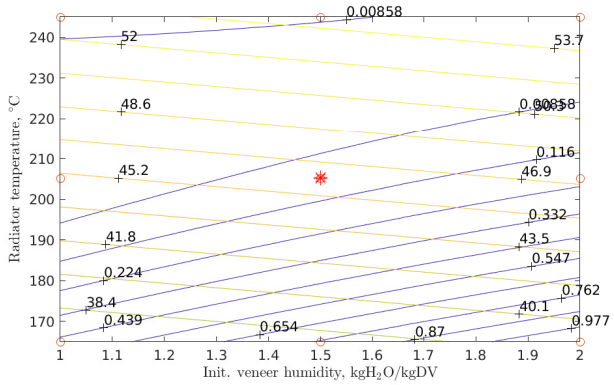

Figure 22: Optimal values and response values for final veneer humidity and power consumption with conveyor speed at 0.045m/s, fan rate at 35m^3/s and atmospheric pressure at 1013hPa.

cells, the heat, removed during the active evaporation, is in balance with the heat transferred from hot air to the veneer. Then, the drying rate is gradually decreased and the veneer temperature rises to 150°C in case 1 and to 180°C in case 3. In the following cooling cells the temperature of the moving veneer drops to 30 – 40°C, is a temperature suitable for manual handling. The mass and energy transport coefficients used in the convective drying model are empirical. The model performance is then compared and discussed. The simulation time is rather short from 10 to 20 minutes at reasonable time step size. The maximum time step size is limited by the air residence time in the fan sub-block.

The tested model shows adequate results obeying the physical principles of the thermodynamics. The validated model was used to optimise the process of convective drying for the veneer sheets. The veneer final moisture content at the end of the simulation was 0.04 $kgH_2O/kgDV$. The complicated mechanisms of heat and mass transfer inside the veneer dryer were simulated in three different scenarios step-wise increasing the model complexity. All three cases showed similar level of drying rate in the drying chambers. However, the simulated case 3, which is the closest to the practical running process, produced the driest veneer sheets and the least air humidity level in the drying chambers.

The selected operational parameters of the continuous veneer drying unit such as initial veneer humidity, radiator temperature, atmospheric pressure, fan speed, and conveyor belt speed were studied within the range of their practical variations via

sensitivity analysis. The simulation outcomes using a balanced full factorial design indicated that the radiator temperature, the initial veneer humidity, and the fan rate were the most crucial parameters for the final veneer humidity output while all parameters except conveyor speed were significant for the power consumption output model. The regression model was used to characterise the relationship between the parameters and the model output. Subsequently, the ANOVA method was used to validate the regression model and a multi-objective optimisation to determine optimal set of parameters for the conflicting objective functions. The first model attains a high final veneer humidity with low radiator temperature and high initial veneer humidity, and a low final veneer humidity with high radiator temperature and low initial veneer humidity while the second model attains a high power consumption with high radiator temperature and high initial veneer humidity and a low power consumption with low radiator temperature and low initial veneer humidity. The multiobjective optimisation was instrumental in combining both objectives of minimising the final veneer humidity and power consumption. The analysis shows how a different combination of input parameters could affect final veneer humidity and power consumption, and the parameters with largest impact identified. The first optimal value for both final veneer humidity and power consumption is 0.03 $kgH_2O/kgDV$ and 38.5 MW at initial veneer humidity of 1.5 $kgH_2O/kgDV$ and radiator temperature of 207.6°C. The second optimal value for both final veneer humidity and power consumption is 0.07 $kgH_2O/kgDV$ and 37.1 MW at initial veneer humidity of 1.5 $kgH_2O/kgDV$ and radiator temperature of 205°C. The results can be used as a guide for the real operational process in the case where a decision marker can select from varying optimal values.

7. Declaration of interests

The authors declare that they have no known competing financial interests or personal relationships that could have appeared to influence the work reported in this paper.

8. Acknowledgement

The authors are grateful to Raute Oyj for the equipment provided and active supervision and financial support.

References

Antony, J. (2014). *Design of Experiments for Engineers and Scientists*. Elsevier.

Aydin, I., & Colakoglu, G. (2005). Formaldehyde emission, surface roughness, and some properties of plywood as function of veneer drying temperature. *Drying Technology*, *23*, 1107–1117.

Baldwin, R. F. (1995). *Veneer Drying and Preparation, In Plywood and Veneer-based Products*. Miller Freeman Books: San Francisco, Calif.

Baxi, H., Patel, A., & Barve, J. (2015). Modelling and simulation of dryer system. In *2015 International Conference on Industrial Instrumentation and Control (ICIC)* (pp. 1544–1549). IEEE.

Bhattacharyya, B. (2018). A critical appraisal of design of experiments for uncertainty quantification. *Archives of Computational Methods in Engineering*, *25*, 727–751.

Borgonovo, E., & Plischke, E. (2016). Sensitivity analysis: a review of recent advances. *European Journal of Operational Research*, *248*, 869–887.

Bose, D., Wright, M. J., & Palmer, G. E. (2006). Uncertainty analysis of laminar aeroheating predictions for mars entries. *Journal of Thermophysics and Heat Transfer*, *20*, 652–662.

Burnaev, E., Panin, I., & Sudret, B. (2017). Efficient design of experiments for sensitivity analysis based on polynomial chaos expansions. *Annals of Mathematics and Artificial Intelligence*, *81*, 187–207.

Cacuci, D. G. (2003). Sensitivity and uncertainty analysis: Theory v. 1: Theory vol 1.

Christiansen, A. (1994). Effect of overdrying of yellow-poplar veneer on physical properties and bonding. *Holz als Roh-und Werkstoff*, *52*, 139–149.

Coello, C. A. C. (2018). Multi-objective optimization. *Journal: Handbook of Heuristics*, (pp. 1–28).

Colbeck, H. M., Hancock, W., Northcott, P., & Canada Dept of Forestry (1962). *Water relations in phenolic (plywood) bonds*.

Cox, D. C., & Baybutt, P. (1981). Methods for uncertainty analysis: a comparative survey. *Risk Analysis*, *1*, 251–258.

Dante, R. C., Escamilla, J. L., Madrigal, V., Theuss, T., de Dios Calderón, J., Solorza, O., & Rivera, R. (2003). Fractional factorial design of experiments for pem fuel cell performances improvement. *International Journal of Hydrogen Energy*, *28*, 343–348.

Demirkir, C., Özsahin, Ş., Aydin, I., & Colakoglu, G. (2013). Optimization of some panel manufacturing parameters for the best bonding strength of plywood. *International Journal of Adhesion and Adhesives*, *46*, 14–20.

Di Marco, P., Frigo, S., Gabbrielli, R., & Pecchia, S. (2016). Mathematical modelling and energy performance assessment of air impingement drying systems for the production of tissue paper. *Energy*, *114*, 201–213.

Ehrgott, M. (2008). Multiobjective optimization. *Ai Magazine*, *29*, 47–47.

Euh, S. E., Choi, Y. S., Nam, Y. S., Lee, C. G., Lee, S. Y., Oh, K. C., Oh, J. H., & Kim, D. H. (2018). Development of a real-time drying control system for a pneumatic conveying dryer for sawdust in pellet production. *Energy*, *161*, 10–16.

Faraway, J. J. (2002). *Practical regression and ANOVA using R*. volume 168. University of Bath Bath.

Gaillemard, C. (2006). *Modelling the moisture content of multi-ply paperboard in the paper machine drying section*. Ph.D. thesis KTH Royal Institute of Technology, Sweden.

Gembicki, F., & Haimes, Y. (1975). Approach to performance and sensitivity multiobjective optimization: The goal attainment method. *IEEE Transactions on Automatic control*, *20*, 769–771.

Gluesenkamp, K. R., Boudreaux, P., Patel, V. K., Goodman, D., & Shen, B. (2019). An efficient correlation for heat and mass transfer effectiveness in tumble-type clothes dryer drums. *Energy*, *172*, 1225–1242.

Hoaglin, D. C., & Welsch, R. E. (1978). The hat matrix in regression and anova. *The American Statistician*, *32*, 17–22.

Jaimes, A. L., Martınez, S. Z., & Coello, C. A. C. (2009). An introduction to multiobjective optimization techniques. *Optimization in Polymer Processing*, (pp. 29–57).

Jamaleddine, T. J., & Ray, M. B. (2010). Application of computational fluid dynamics for simulation of drying processes: A review. *Drying Technology*, *28*, 120–154.

Jia, L., Chu, J., Ma, L., Qi, X., & Kumar, A. (2019). Life cycle assessment of plywood manufacturing process in china. *International Journal of Environmental Research and Public Health*, *16*, 2037.

Johnsson, S., Andersson, E., Thollander, P., & Karlsson, M. (2019). Energy savings and greenhouse gas mitigation potential in the swedish wood industry. *Energy*, *187*, 115919.

Kalyanaraman, J., Fan, Y., Labreche, Y., Lively, R. P., Kawajiri, Y., & Realff, M. J. (2015). Bayesian estimation of parametric uncertainties, quantification and reduction using optimal design of experiments for co2 adsorption on amine sorbents. *Computers & Chemical Engineering*, *81*, 376–388.

Kleijnen, J. P. (1995). Sensitivity analysis and optimization of system dynamics models: regression analysis and statistical design of experiments. *System Dynamics Review*, *11*, 275–288.

Kleijnen, J. P. (2005). An overview of the design and analysis of simulation experiments for sensitivity analysis. *European Journal of Operational Research*, *164*, 287–300.

Lakshmanan, A., & Claus, R. (2013). Modeling solids dryers and granulators with aspen plus v8. *Aspen Technology*, .

Lamrani, B., Kuznik, F., Ajbar, A., & Boumaza, M. (2021). Energy analysis and economic feasibility of wood dryers integrated with heat recovery unit and solar air heaters in cold and hot climates. *Energy*, *228*, 120598.

Laurijssen, L., De Gram, F. G., Worrell, E., & Faaij, A. (2010). Optimizing the energy efficiency of conventional multi-cylinder dryers in the paper industry. *Energy*, *35*, 3738–3750.

Lin, G., Engel, D. W., & Eslinger, P. W. (2012). *Survey and Evaluate Uncertainty Quantification Methodologies*. Technical Report Pacific Northwest National Lab.(PNNL), Richland, WA (United States).

Mujumdar, A. S. (2014). 15 impingement drying. *Handbook of Industrial Drying*, (p. 371).

Ozsahin, S., & Aydin, I. (2014). Prediction of the optimum veneer drying temperature for good bonding in plywood manufacturing by means of artificial neural network. *Wood Science and Technology*, *48*, 59–70.

Politis, S., Colombo, P., Colombo, G., & M. Rekkas, D. (2017). Design of experiments (doe) in pharmaceutical development. *Drug Development and Industrial Pharmacy*, *43*, 889–901.

Radmanović, K., Đukić, I., & Pervan, S. (2014). Specific heat capacity of wood. *Drvna industrija: Znanstveno-stručni časopis za pitanja drvne tehnologije*, *65*, 151.

Rouch, H. (2010). Fluid flow simulations using new cfd module – wood drying simulation. In *Proceedings of the COMSOL Conference Paris: 1–4*.

Sałat, R., Awtoniuk, M., & Korpysz, K. (2017). Black-box identification of a pilot-scale dryer model: A support vector regression and an imperialist competitive algorithm approach. *IFAC-PapersOnLine*, *50*, 1559–1564.

Saltelli, A., Ratto, M., Andres, T., Campolongo, F., Cariboni, J., Gatelli, D., Saisana, M., & Tarantola, S. (2008). Introduction to sensitivity analysis. *Global sensitivity analysis. The primer*, (pp. 1–51).

Sandoval Torres, S., Jomaa, W., Puiggali, J.-R., & Avramidis, S. (2011). Multiphysics modeling of vacuum drying of wood. *Applied Mathematical Modelling*, *35*, 5006–5016.

Smit, G., Du Plessis, J., & du Plessis Sr, J. (2007). Modelling of airflow through a stack in a timber-drying kiln. *Applied Mathematical Modelling*, *31*, 270–282.

Steven, F., Bruning, P., & Fellow, A. (2004). Fundamental handbook. (pp. 20–24). ASHRAE volume 46.

Thant, A., Yee, S., & Htike, T. T. (2009). Modeling drying time during veneer drying and comparison with experimental study. In *Proceedings of the International Multiconference of Engineers and Computer Scientists. Hong kong*.

Welty, J., Rorrer, G. L., & Foster, D. G. (2020). *Fundamentals of Momentum, Heat, and Mass Transfer*. John Wiley & Sons.

Woods, D., & Lewis, S. (2017). Design of experiments for screening, .

Zhang, J., Yin, J., & Wang, R. (2020). Basic framework and main methods of uncertainty quantification. *Mathematical Problems in Engineering*, *2020*.

Appendix

Operational conditions and constants used in calculations	Values	Units
Air flow rate at the fan	25	m^3/s
Static pressure at 20°C	0.005	Pa $m^3/(kg°C)$
Temperature of atmosphere	20	°C
Radiator temperature	205	°
Humidity of air in atmosphere	80	%
Dryer production capacity	6	kg/s
Initial humidity of veneers	1.5	$kgH_2O/kgDV$
Veneer thickness	3.3×10^{-3}	m
Veneer size (square plates)	1.4	m
Speed of veeners transport	0.055	m/s
Convective heat transfer coefficient	50	$W/(m^2°C)$
Total contact area of veneers at a cell	100	m^2
Number of missing veneers (not specified)	0	$(m^2\text{tray})^{-1}$
Conveyor load (not specified)	0	$(m^2\text{tray})^{-1}$
Atmospheric pressure	101300	Pa
Mass transfer	3.26×10^{-4}	m/s
Density of dry veneer	430	kg/m^3
Heat capacity of water vapour	1900	$J/(kg°C)$
Heat capacity of veneer (Radmanović et al., 2014)	1340	$J/(kg°C)$
Heat capacity of dry air	1000	$J/(kg°C)$
Heat capacity of water	4200	$J/(kg°C)$
Heat capacity of stainless steel	500	$J/(kg°C)$
Molar mass of water	18	g/m
Latent heat of water	2.26×10^6	J/kg
Convective mass transfer	5.6×10^{-4}	m/s
Density of dry air	0.63	kg/m^3
Density of dry veneer	430	kg/m^3
Kinematic viscosity of air	1.48×10^{-5}	m^2/s
Diffusivity of vapour through veneer	2.7×10^{-5}	m^2/s
Free parameter $k^{(-1/2)}$ in PID controllers	0.025-35	-

Table .9: Parameters used in the simulations of the veneer dryer.